scientific reports

Check for updates

OPEN

High-efficiency upconversion process in cobalt and neodymium doped graphene QDs for biomedical applications

Armin Zarghami[1], Mahboubeh Dolatyari[2], Hamit Mirtagioglu[3] & Ali Rostami[1,2]✉

Multiphoton absorbing upconversion nanoparticles are emerging as bioimaging materials but are limited by the low quantum yield of their visible fluorescence. This article contains colloids of graphene quantum dots (GQDs), Neodymium, and Cobalt doped Graphene Quantum dots (Co-GQDs and Nd-GQDs) surrounded by carboxylic acids are synthesized which especially are suitable for bio applications; in this way, carboxylic acid groups exchanged by Amoxicillin as an antibiotic with bactericidal activity. The XRD diffraction method, TEM microscope, UV–Vis, and photoluminescence spectroscopies characterize the synthesized materials. The synthesized Quantum dots (QDs) exhibit upconversion properties and their emission is centered at 480 nm, but a red shift was observed with the increase of the excitation wavelength. In the emission spectra of synthesized QDs that can be related to the defect levels introduced by passivation of the QDs in the structure, the results show that with the interaction of the surface QDs with more carboxylic groups, the redshift is not observed. As the results indicate an increase in the intensity of upconversion emission is recorded for Co-GQDs and Nd-GQDs. The absolute quantum efficiency (QY) for Co-GQDs and Nd-GQDs were determined to be 41% and 100% more than GQDs respectively. DFT calculations indicate a strong bond between graphene and cobalt and Neodymium atoms. In doped materials, there are trap levels between the band gap of the GQDs which are responsible for increasing the intensity of the upconversion phenomenon.

In recent years, graphene quantum dots (GQDs) have attracted much attention due to their unique structural and optoelectronic properties and their great potential in various applications in drug delivery[1–5], sensors[6–12], bio-imaging[13–18], magnetic hyperthermia[19–21], photothermal therapy[22–26], antibacterial[23–28], catalyst[29–33], environmental protection[34,35], energy conversion, spintronics, photovoltaic devices[36–53] has made a remarkable accomplishment. One of the important features of these nanoparticles is having high fluorescence properties that can be used for biological imaging and optical sensing. GQDs have attracted much attention as promising biomaterials due to their exceptional advantages of low cytotoxicity, excellent solubility, stable photoluminescence (PL), biocompatibility, and low cost[54–59].

Conventional imaging probes, such as fluorescent dyes and fluorescent proteins, have attracted much attention. However, they face poor diagnostic sensitivity, instability, and high toxicity and have no therapeutic effect. It was difficult to find a dual-purpose material that could act as an imaging probe and a drug delivery at the same time. As an effective drug delivery, the fluorescent matrix should meet the following criteria: (1) effective drug delivery, (2) good biocompatibility, and (3) good circulation stability in vivo[60–63]. Recently, the rapid development in nanomedicine has opened a new way to find such materials, and nanomaterials have become a very important topic in biomedical applications due to their great potential for the formulation of anticancer drugs. Engineered nanomaterials that have the effect of permeability, biocompatibility, and low toxicity can be used in biomedical applications, including biomedical diagnosis and disease treatment[64,65].

Up conversions, nanoparticles (UCNPs) have anti-Stokes luminescence that can convert near-infrared (NIR) light into visible light. UCNPs have high chemical stability and can be used as fluorescence probes in a variety of complex organisms and facilitate the bioassay process. In addition, UCNPs can lead to surface conjugation with specific targeting ligands (such as peptides, antibodies, and small molecule drugs) and can be used as probes to

[1]Photonics and Nanocrystal Research Lab. (PNRL), University of Tabriz, Tabriz 5166614761, Iran. [2]SP-EPT Lab., ASEPE Company, Industrial Park of Advanced Technologies, Tabriz, Iran. [3]Department of Statistics, Faculty of Science and Literature, University of Bitlis Eren, Bitlis, Turkey. ✉email: rostami@tabrizu.ac.ir

identify and target specific cells with high sensitivity and selectivity[66,67]. Lanthanide-doped materials are among the most well-known UCNPs in which trivalent lanthanide ions are dispersed as guests in a suitable host network with dimensions less than 100 nm. Lanthanide impurities are photoactive centers that emit light after excitation with low-energy photons. Through a suitable selection of lanthanide dopants, UCNPs can exhibit selective wavelength (color) conversion such as NIR to shorter NIR, visible (blue, green, red), or UV[68].

UCNPs are an improved alternative to traditional optical imaging materials due to several other advantages, such as weak photobleaching, low background fluorescence, deep tissue penetration, and minimal photodamage[69–73]. In addition, as a new generation of imaging agents, UCNPs are widely used in PDT, MRI, X-ray CT imaging, photoacoustic imaging (PA), NIR thermal imaging, phototherapy (PTT), chemotherapy, and radiotherapy. Increasingly studies have focused on their application in PDT because they can act as a photosensitizer in photodynamic therapy[74–79]. Also, they can be used as drug carriers for bioimaging therapeutic drugs or genes (such as doxorubicin, siRNA, DNA, and microRNA) or light-sensitive materials. More importantly, UCNP in antibacterial photodynamic therapy (aPDT) has played an essential role in the treatment of bacterial infectious diseases, such as periodontitis and Staphylococcus aureus infections, which are incurable and difficult to eradicate[80]. The development of nanomaterials that exhibit both good upconversion luminescence (UCL) performance and good performance is undoubtedly a challenge for materials scientists, physicists, and chemists.

Surface modification of nanoparticles is usually necessary to create a suitable surface composition for biomedical applications[81]. For example, surface modification of UCNPs is important for loading some hydrophobic drugs, and surface charge for the adsorption of small molecules[82]. However, different needs make different changes, and careful design and optimization of these aspects are necessary before using UCNPs for bioanalytical applications[83].

Bioconjugation of UCNP materials with biomolecules is very important in therapeutic and diagnostic applications. Recent research has shown that surface-modified ligands on UCNPs can be transformed into a new functional group to influence the subsequent bioconjugation step. Ligands commonly used for coupling are maleimides[84], thiols[85], carboxylic acids[86], aldehydes, and amine groups.

Compared with traditional medicine, UCNP-based drug delivery has obvious advantages such as small particle size, which facilitates the endocytosis of cells to obtain a good therapeutic effect[60]. The large surface area of UCNPs can prolong the shelf life of topical drugs and enhance the use of drug targeting in tissues[87,88]. Even better, UCNP-based composites used as drug delivery systems allow real-time tracking and evaluation of drug release efficiency[89,90].

Graphene-based nanomaterials have been designed to help deliver or target drugs more effectively. They are being investigated for therapeutic applications, especially for cancer treatment, as well as for the development of new diagnostics and nanosensors, and are expected to contribute to molecular imaging for diagnosis and treatment, especially in the development of therapeutic strategies in oncology[91–93].

In this article, colloidal graphene nanoparticles doped with cobalt and neodymium cations were designed and synthesized with the aim of biological imaging. The surface of nanoparticles is decorated by carboxylic groups that can be bioconjugated with biomolecules. Here our goal is to increase the quantum yield of the upconversion property of the graphene quantum dots by doping cobalt and neodymium ions in their structure. The results show a 41% increase for cobalt and a 100% increase for neodymium-doped graphene in the intensity of the upconversion phenomenon. The mentioned structures were simulated using DFT calculations and their electronic properties were obtained.

Materials and method

Chemicals. All chemicals purchased from Merck Company and used as received.

Synthesis of cobalt-doped GQDs. The GQDs and Co-doped GQDs were prepared by the thermal decomposition of citric acid (CA). In a typical procedure of GQDs preparation, 2 g CA and, 0.1 g of the cobalt acetate was put into a 50 mL beaker and heated to 200 °C using a heating mantle. About 5 min later, the CA was liquated. Subsequently, the color of the liquid was changed from colorless to pale yellow, and then orange in 30 min, implying the formation of GQDs. The obtained orange liquid for preparing GQDs was added drop by drop into 100 mL of 10 mg mL^{-1} NaOH solution, under vigorous stirring. After neutralizing to pH 7.0 with NaOH, the aqueous solution of GQDs was obtained[94]. For synthesis, Nd-doped Graphene cobalt acetate was substituted by Neodymium acetate. The obtained synthesized materials were centrifuged and washed with water for 1 h at 12,000 rpm and redispersed in deionized water.

Exchanging amoxicillin (6-[D(−)β-amino-p-hydroxyphenyl-acetamido]) with surface carboxylic acids. 0.5 g of Amoxicillin was solved in 10 CC of deionized water and dropwise added on 20 CC of the synthesized colloids and stirred for 2 h. The obtained exchanged materials were centrifuged and washed with water for 1 h at 12,000 rpm and redispersed in deionized water.

Characterization. The size and shape of synthesized nanoparticles were measured at ×200–×300 magnifications using TEM microscopy imaged by a Zeiss-EM10C TEM microscope at 80 kV accelerating voltage and ~2 nA beam current. The EDX analysis was employed to identify the elemental composition of the nanoparticles. UV–Vis absorption spectra were recorded employing a PG Instruments Ltd T70 UV/Vis spectrophotometer. PL spectra were taken by a Perkin Elmer LS-45 spectrophotometer equipped with a 500 W Xenon lamp. For lower powers, we used an optical filter in front of the instrument's source. ICP analysis was recorded by ICP-OES SPECTRO ARCOS. Powder X-ray diffraction patterns were recorded by XRD Bruker D8 advance.

DFT simulations. The Gaussian 03 package and materials studio CASTEP model was applied for DFT calculation. The electronic structures were established based on Graphene nanoclusters containing 54 carbon atoms passivized by carboxylic groups and bonded with Cobalt acetate surrounded by H_2O molecules. B3LYP/6-311G (d,p) basis sets and LDA approximation were used in the geometry optimizations. In the CASTEP, calculation, the number of plane waves included in the basis was determined from cut-off energy (*Ec*) of 500.0 eV. The summation over the Brillouin zone was carried out with *k*-point sampling using a Monkhorst–Pack grid. Geometry optimization under applied hydrostatic pressure with parameters of $2 \times 2 \times 5$ was used to determine the modulus of a material (B) and its pressure derivative, $B' = dB/dP$[95].

Results and discussion

Figure 1 shows the TEM image of the synthesized GQDs and their doping with cobalt and Neodymium ions with a diameter of 10 nm. As the figure shows the shape and size of quantum dots are nearly the same for all materials.

X-ray diffraction shows that no peak related to cobalt and Nd ions can be seen and only there are small shifts in the appeared peaks in the related patterns, which indicates the doping of ions in the structure of the graphene quantum dot. The peaks appeared at $2\theta = 24°$ along the (002) orientation and $2\theta = 43°$ according to (102) orientation indicating synthesizing GQDs (see Fig. 2). As the figure shows crystallinity in doped graphenes is less than in undoped Graphene.

ICP measurements indicate 10 and 12 ppm Co and Nd ions in the colloidal sample respectively.

Figure 3 shows calculated absorption spectra for GQDs, Co-GQDs, and Nd-GQDs. As Fig. 3A shows there are peaks centered at 74.3, 179.6, and 281.2 nm for GQDs, and in wavelengths, upper than 400 nm the absorption intensity is zero. For Co-doped graphene QDs, the observed peaks are at 75.56, 106.6, and 315 nm, and 74.02, 107.3, and 220.6 nm for Nd-doped QDs. Also in doped materials, there is absorption at wavelengths upper than 400 nm. This means there are created trap electronic levels between the band gap of the graphene after doping cobalt and neodymium ions in the structure of graphene.

The absorption spectra of synthesized GQDs, Co-GQDs, and Nd-GQDs show two absorption bands. The first peak for Graphene is at 211.11 nm and the second one is at 324.4 nm (Fig. 4A). The first peak for Co-doped graphene is at 244 nm and the second peak is at 338.9 nm (Fig. 4B). The first peak for Nd is at 250 nm and the second is at 331.1 nm (Fig. 4C). The peaks are relatively broad and we can't recognize other peaks related to electronic levels of Co and Nd ions. Shifts in both peaks can be related to differences in the radius of doped ions and the effect on the electronic structure of Graphene. A comparison of the GQDs without Cobalt atoms indicates that the intensity of the peak at 350 nm is high in cobalt-doped graphene. Also, the absorption intensity in wavelengths upper than 400 nm is not zero for doped synthesized materials.

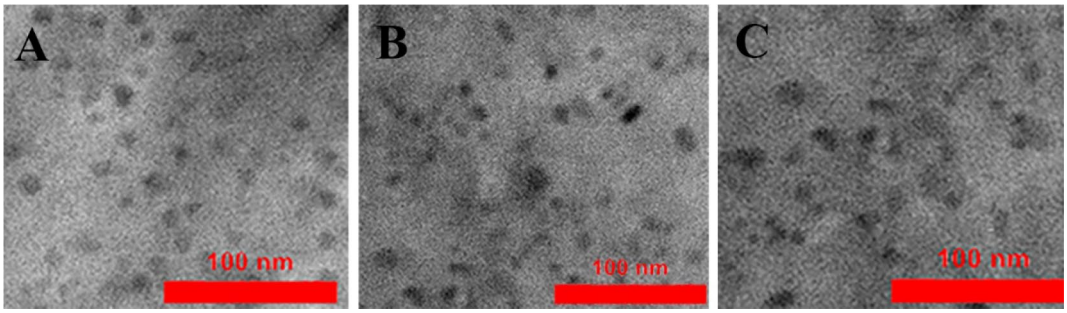

Figure 1. TEM image of the synthesized (**A**) GQDs (**B**) Co-GQDs (**C**) Nd-GQDs.

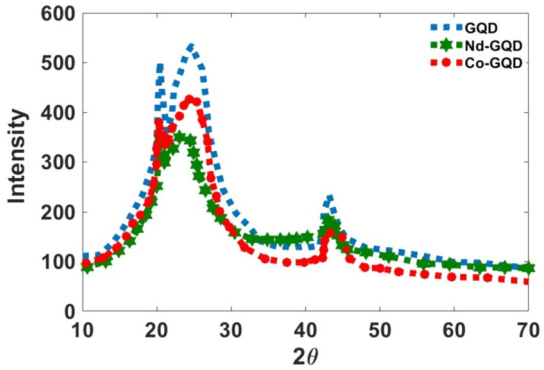

Figure 2. The XRD diffraction pattern for synthesized CO-Graphene and Nd-Graphene quantum dots.

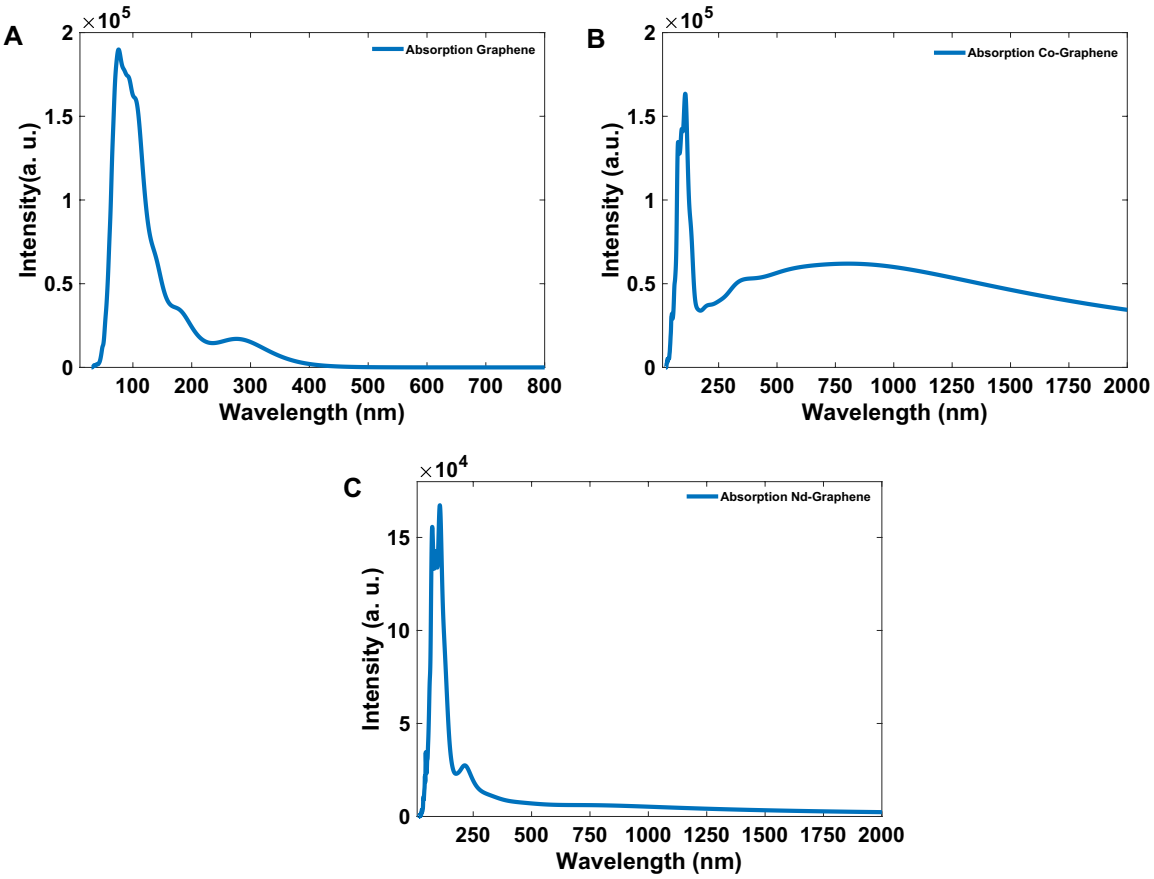

Figure 3. Calculated absorption spectra of (**A**) GQDs, (**B**) CO-GQDs, and (**C**) Nd-GQDs.

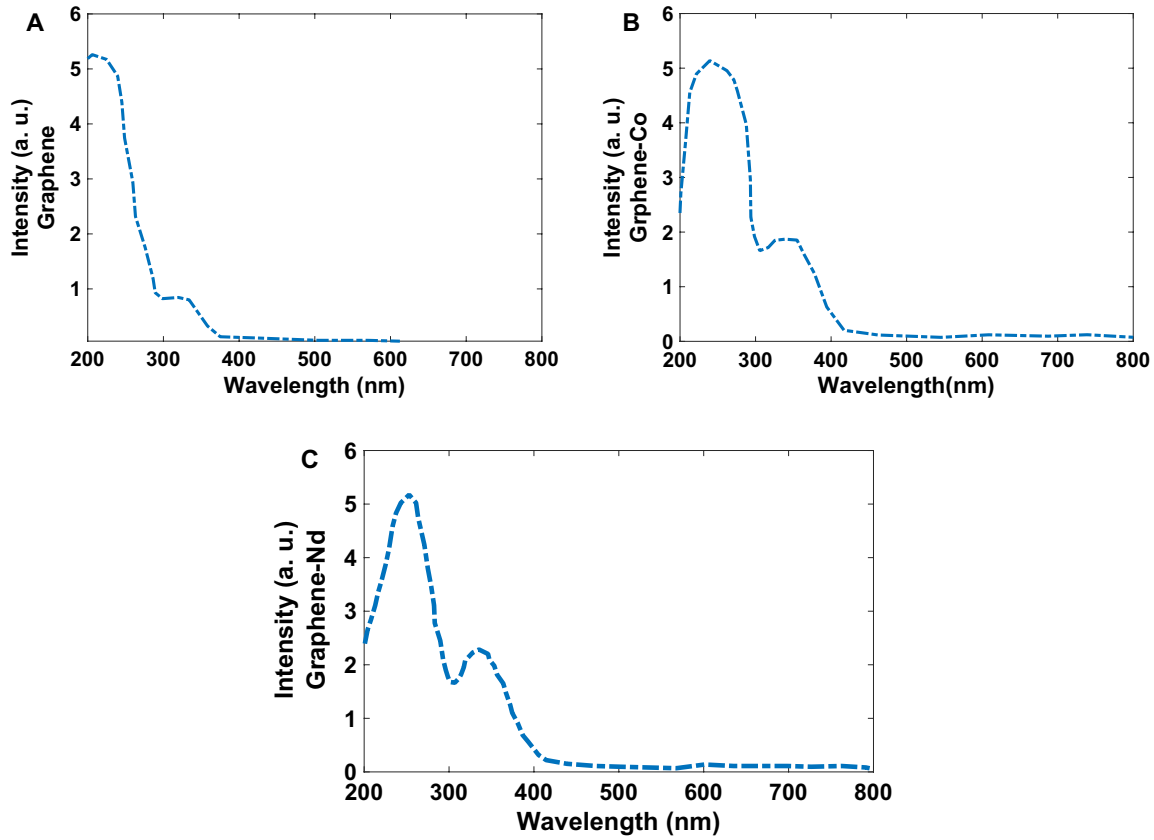

Figure 4. Absorption spectra of (**A**) GQDs, (**B**) Co-GQDs, and (**C**) Nd-GQDs.

To further investigate the optical properties of the synthesized GQDs, a detailed PL study was performed using different excitation wavelengths. In general, the PL spectrum of graphene nanoparticles depends on the excitation wavelength. In other words, the PL peaks shift to longer wavelengths of maximum intensity because the excitation wavelength is a bathochromic shift[96]. Shen et al.[97] have reported that the linear relationship between E_m and E_x, and the function of the fit line is $E_m = 1.00E_x + \delta E$ ($R^2 = 0.9983$) with $\delta E = 1.1$ eV. All these changes come from the surface passivation of nanoparticles (in our case citrate ligands) that strongly influence the optical properties of the GQDs and trap states created by surface defects of the structure.

The photoluminescence emission spectrum of the synthesized Co-GQDs and GQDs at 350 and 400 nm excitation wavelengths are presented in Fig. 5. The observed emission bands for both synthesized GQDs and Co-GQDs are at 450 and 480 nm (excitation wavelengths are 350 and 400 nm). Also, a decreasing trend in emission intensity values was observed with increasing excitation wavelength.

As the figure shows, the intensity of photoluminescence in Graphene is relatively higher than Co-GQDs because of inserted trap levels by doping Co atoms (it will be described more in the mechanism section).

To prove and correct this phenomenon, the surface of nanoparticles was modified with excess citric acid (how to do the work is explained in the materials and methods section). As Fig. 6 shows, nanoparticles modified with citric acid do not show any frequency shift at 350 and 400 nm excitation, and the emission peak is observed at 500–550 nm.

In addition to the PL features, significant upconversion is observed for the synthesized Co-GQDs and Nd-GQDs. Figure 7 shows the PL spectra of the GQDs, Co-GQDs, and Nd-GQDs synthesized nanoparticles excited by long-wavelength light at 650, 700, 750, and 800 nm. The PL spectra show a strong peak centered at 525 nm for both GQDs and Co-GQDs with an excitation wavelength of 800 nm. For Nd-GQDs, there is a strong peak at 500 nm and a shoulder centered at 530 and 600 nm that can be attributed to the electronic transition from $^4G_{7/2} + {}^2K_{13/2}$ and $^2G_{7/2} + {}^4G_{5/2}$ to $^4I_{9/2}$ respectively[98]. As the figure shows an increase in the intensity of PL spectra is recorded for Co-GQDs and the absolute quantum efficiency (QY) for Co-GQDs, and Nd-GQDs were determined to be respectively 41% and 100% more than Graphene QDs. As Fig. 7B,D,F show, binding a biomolecule (Amoxicillin) on the surface of synthesized nanoparticles decrease the intensity of upconversion emission; however, this increase is negligible and the synthesized materials can act as drug delivery compounds.

The upconversion effect of nanoparticles was examined by different power sources (Fig. 8). The obtained PL spectra indicate with the decrease in power source the same bands with lower intensity are observable.

Figure 9 shows the up-and-down conversion effect of synthesized Nd-QDs under the excitation of a laser with a wavelength of 750 nm and an LED with a wavelength of 400 nm.

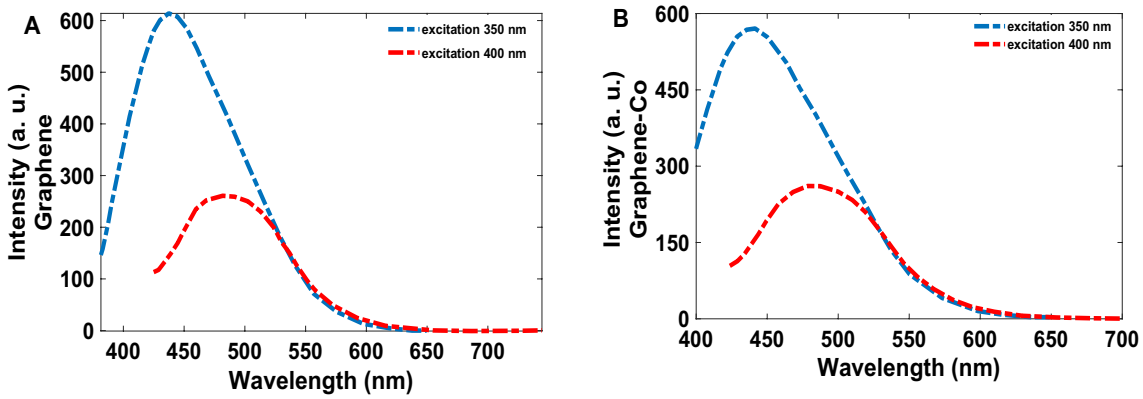

Figure 5. PL spectra of (**A**) GQDs and (**B**) Co-GQDs, excited at 350, and 400 nm.

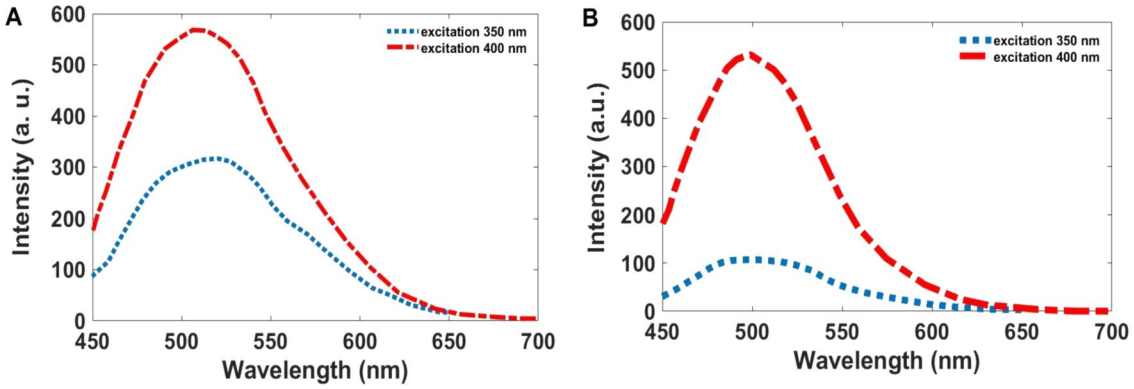

Figure 6. PL spectra of (**A**) GQDs and (**B**) Co-GQDs (surface-modified particles), excited at 350, and 400 nm.

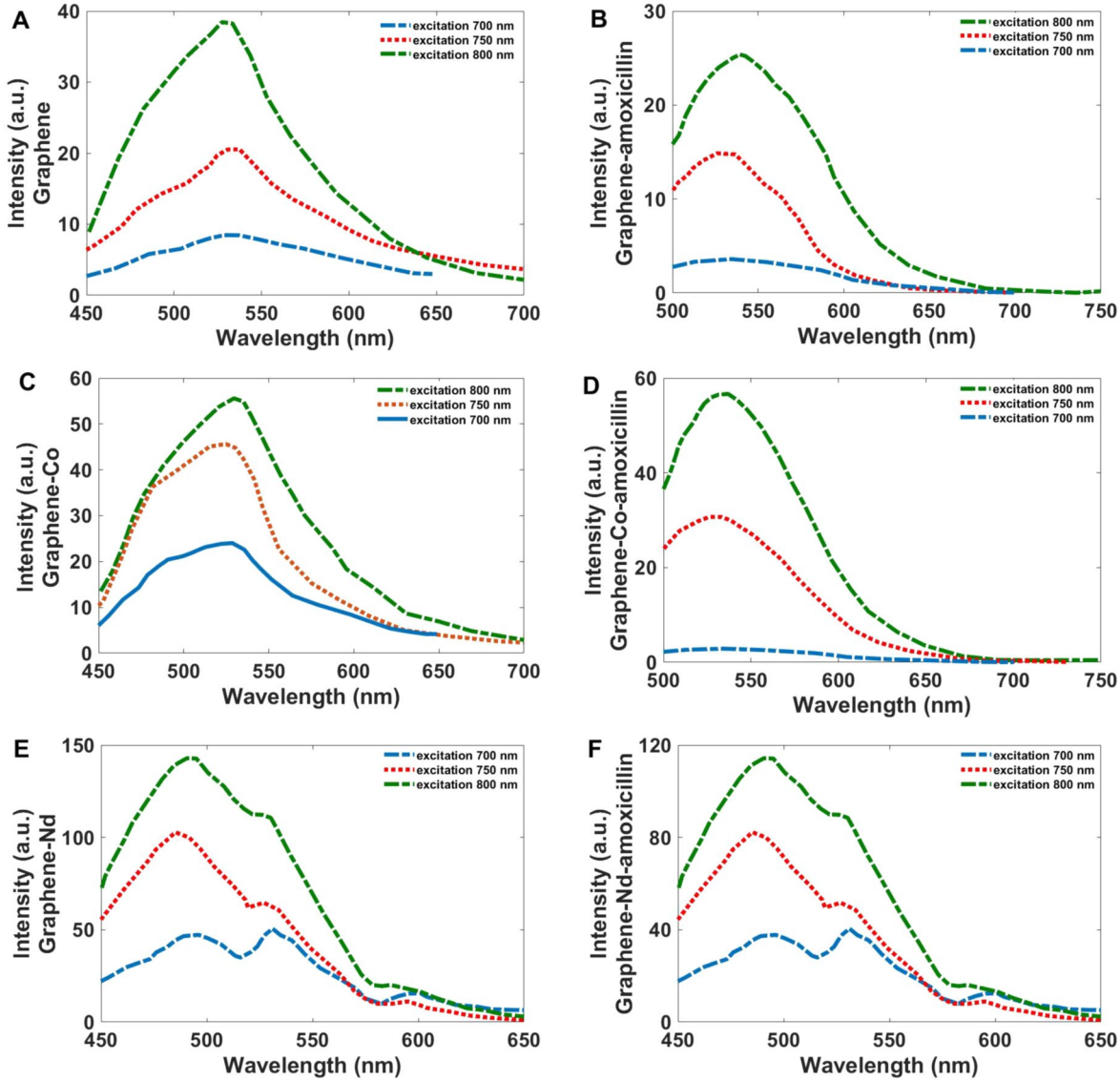

Figure 7. PL spectra of (**A**) GQDs, (**B**) Co-GQDs, and (**C**) Nd-GQD, excited at 700, 750, and 800 nm.

Mechanism of upconversion transition. A simplified energy diagram of optical transition states for cobalt and Neodymium doped graphene structure to illustrate the upconversion mechanism is shown in Scheme 1. As shown in the figure, the presence of levels between HOMO and LUMO in graphene is introduced by doped atoms in the electronic structure and they are related to the unfilled *d* orbitals of Cobalt ions and *f* orbitals related to Neodymium, allowing the absorption of photons with lower energy. It means that absorbing multi-photons with lower energy can excite electrons in multi-steps, which increases the intensity of upconversion emission in cobalt-doped graphene. These trap levels can also reduce the intensity of photoluminescence emission (excitation wavelengths: 350 and 400 nm) in doped quantum dots and increase non-radiative transitions in this structure.

HOMO/LUMO calculations. Figure 10 illustrates HOMO/LUMO orbitals of the Cobalt doped graphene sheet (G) which was computed at B3LYP/6-31G(*d*,*p*) theoretical level. HOMO/SOMO/LUMO orbitals of the Cobalt doped graphene sheet, show highly symmetric configurations indicating the homogeneity of electronic distribution through these orbitals either in the ground states on carbon atoms of the graphene sheet. However, they present asymmetric distribution for SOMO and LUMO, and orbitals are nearly concentrated around the Graphene's added Cobalt atoms and carboxylic acid groups.

Calculated band structures for GQD, Co-GQD, and Nd-GQD are presented in Fig. 11. This figure indicates that the band gap energy for GQD is 2.41 eV (514 nm), which agrees well with experimental results. After doping Cobalt and Neodymium some electronic bands are created between the band gap. These levels are denser in Neodymium doped Graphene.

The density of states (DOS) in Fig. 12 shows that there is a big difference between intrinsic graphene and the Co and Nd doped graphene between 0 and 2 eV. Figures 13, 14 and 15 illustrate the contribution of orbitals in electronic transitions for GQD, Co-GQD, and Nd-GQD.

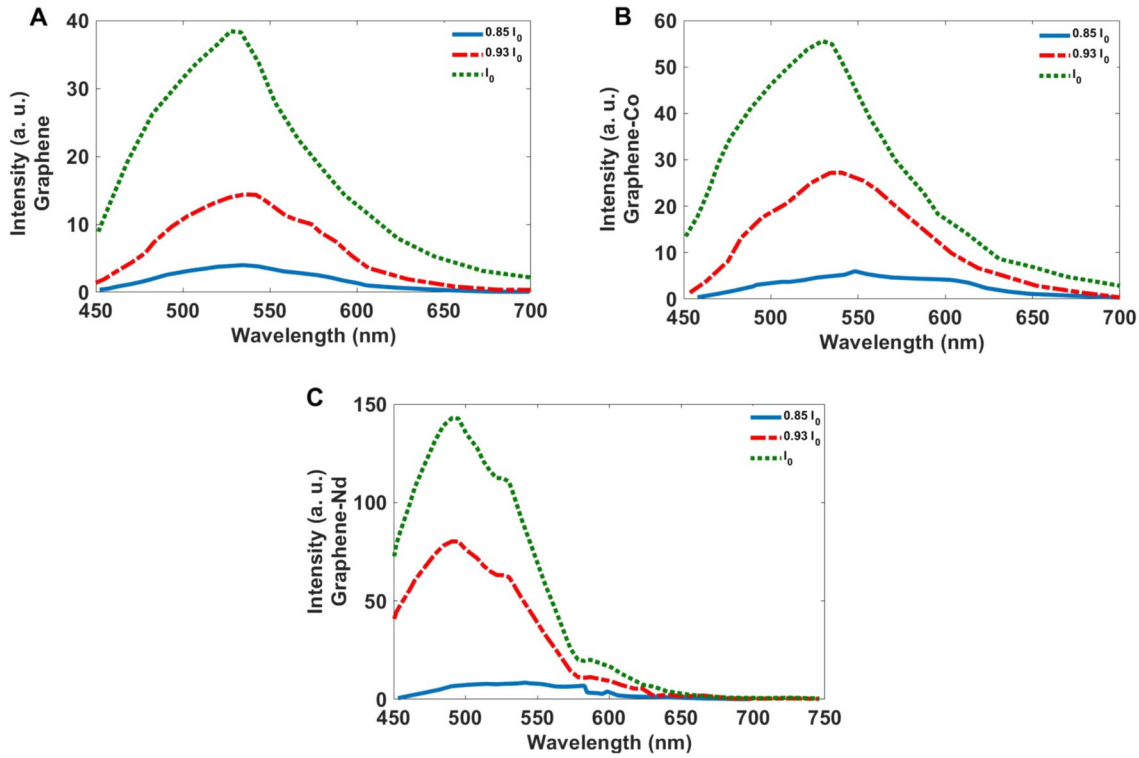

Figure 8. PL spectra of (**A**) GQDs, (**B**) Co-GQDs, and (**C**) Nd-GQD, excited 800 nm for a source with the power of I_0, $I_0/2$, $I_0/3$.

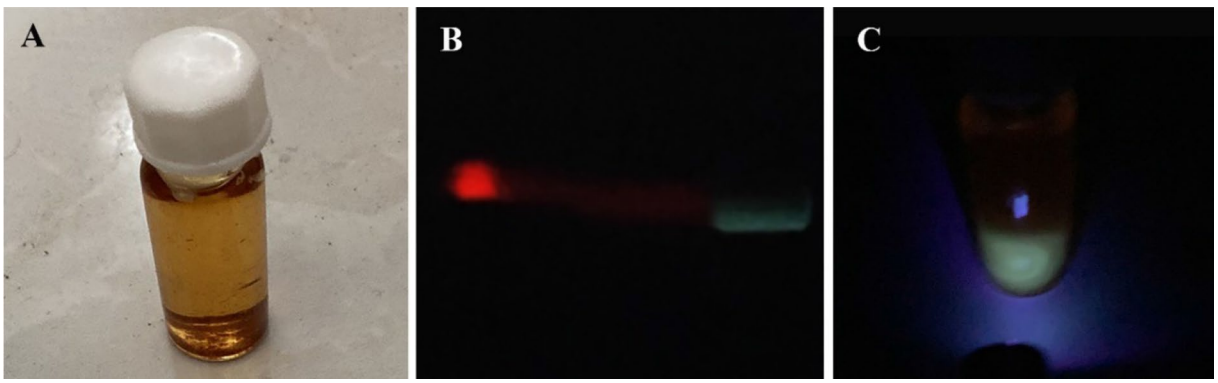

Figure 9. Up and down conversion effect for synthesized Nd-GQD (**A**) synthesized Nd-GQDs (**B**) Nd-GQD under excitation of a laser with wavelength 750 nm, 1w (**C**) Nd-GQD under LED with wavelength 350 nm, 1mw.

As described above, there are carboxylic groups around Graphene QDs and we calculated the partial density of states for C and O atoms. As Fig. 13 shows the *p* orbitals of C and O atoms are attributed to the electronic transitions of GQDs.

Figure 14 indicates the *p* orbitals of the C and O atoms also, the *p* and *d* orbitals of the Co atoms have the most contribution to electronic transitions of Co-GQD. For Nd-GQD (Fig. 15), the *p* orbitals of C and O atoms also *f* orbitals of Nd atoms have a high contribution to the electronic transitions.

Conclusion

In this article, the colloids of Graphene, Graphene-cobalt, and Graphene-Neodymium quantum dots decorated by carboxylic groups were synthesized for bio-imaging purposes and their physical properties were characterized. X-ray diffraction results show that cobalt and Neodymium were doped in the graphene structure and DFT calculations confirm that a strong bond was formed between doped atoms and graphene passivized by citrate. Also, the PL spectra indicate the existence of trap levels between HOMO and LUMO levels of Graphene QDs created by doped atoms in the structure. In this condition, multi-photons with lower energies can excite the electrons and the upconversion transitions can be done with higher intensity. As the results show with doping

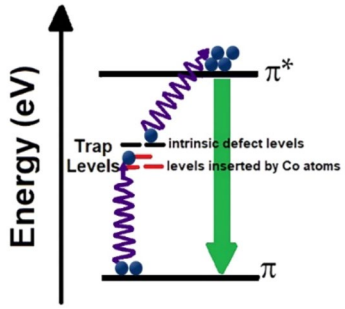

Scheme 1. A simple energy diagram of optical transition states for illustrating the upconversion phenomenon in the synthesized Co-GQDs and Nd-GQDs.

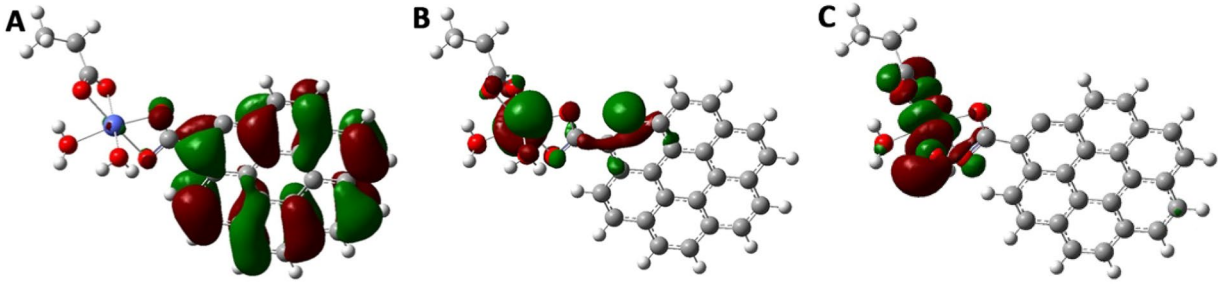

Figure 10. DFT Calculated (**A**) HOMO (**B**) SOMO (**C**) LUMO molecular orbitals of the synthesized Co-GQDs.

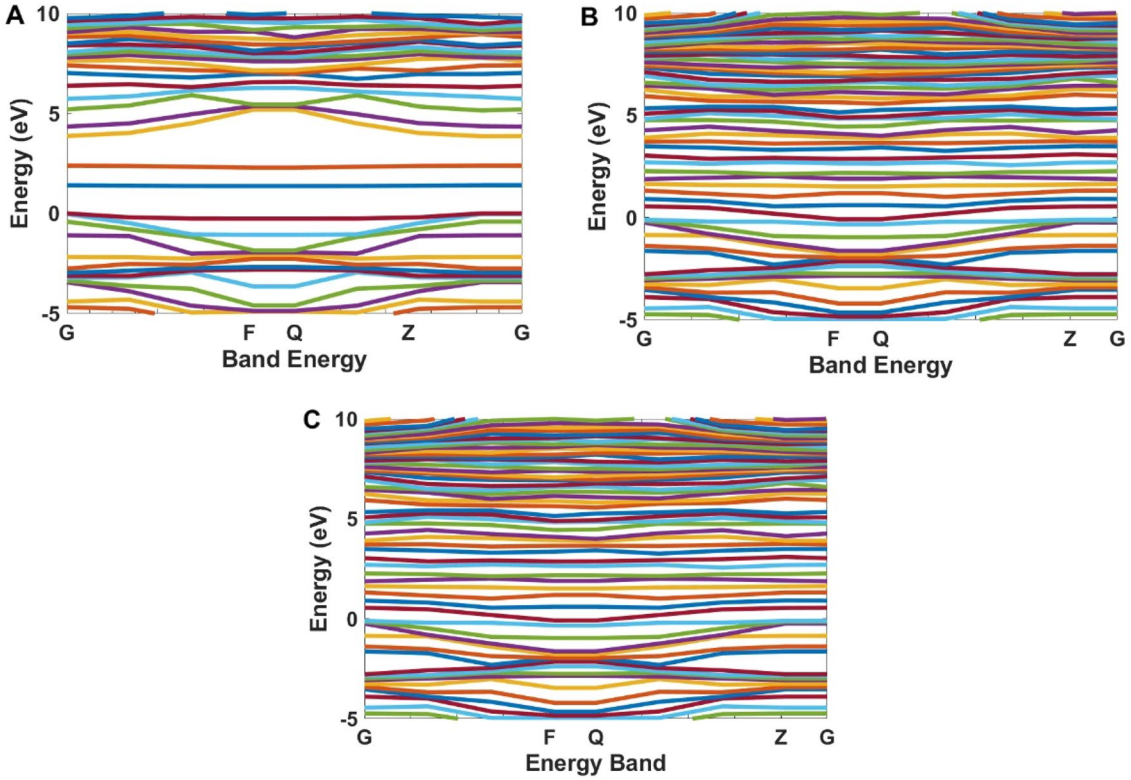

Figure 11. Band structure calculation for (**A**) GQDs, (**B**) Co-GQDs, and (**C**) Nd-GQD.

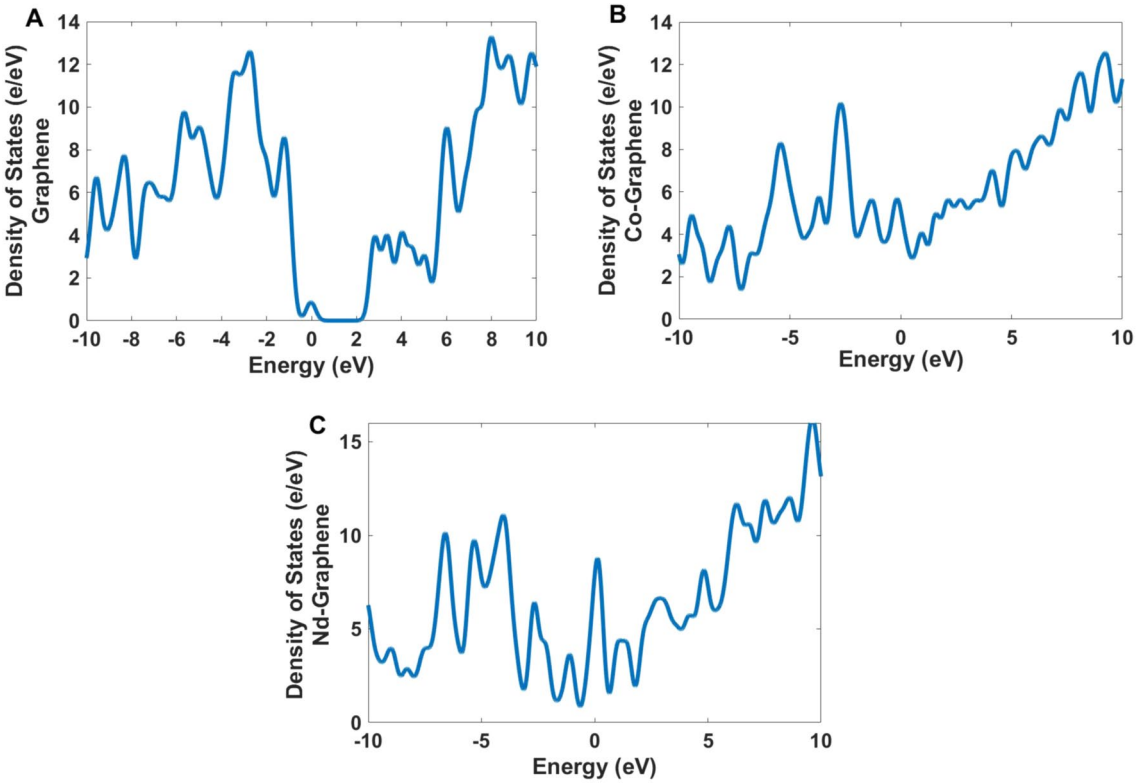

Figure 12. The density of States for (**A**) GQDs, (**B**) Co-GQDs, and (**C**) Nd-GQD.

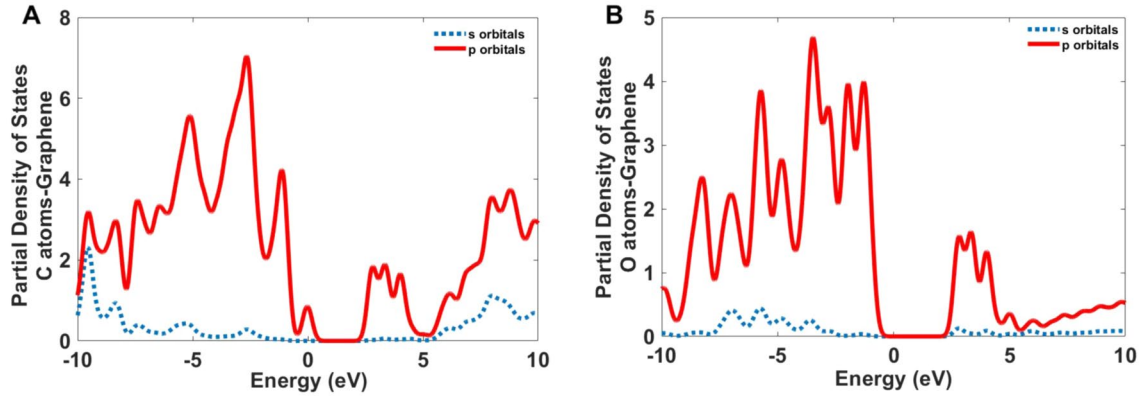

Figure 13. The partial density of states for the C and O atoms of the GQDs.

cobalt and neodymium atoms in the structure of graphene, upconversion intensity can be increased to 41% and 100% more than un-doped graphene. By exchanging the carboxylic groups on the surface of synthesized nanoparticles with Amoxicillin as an antibiotic molecule the upconversion property remains and therefore they can use as drug delivery materials in bio-applications.

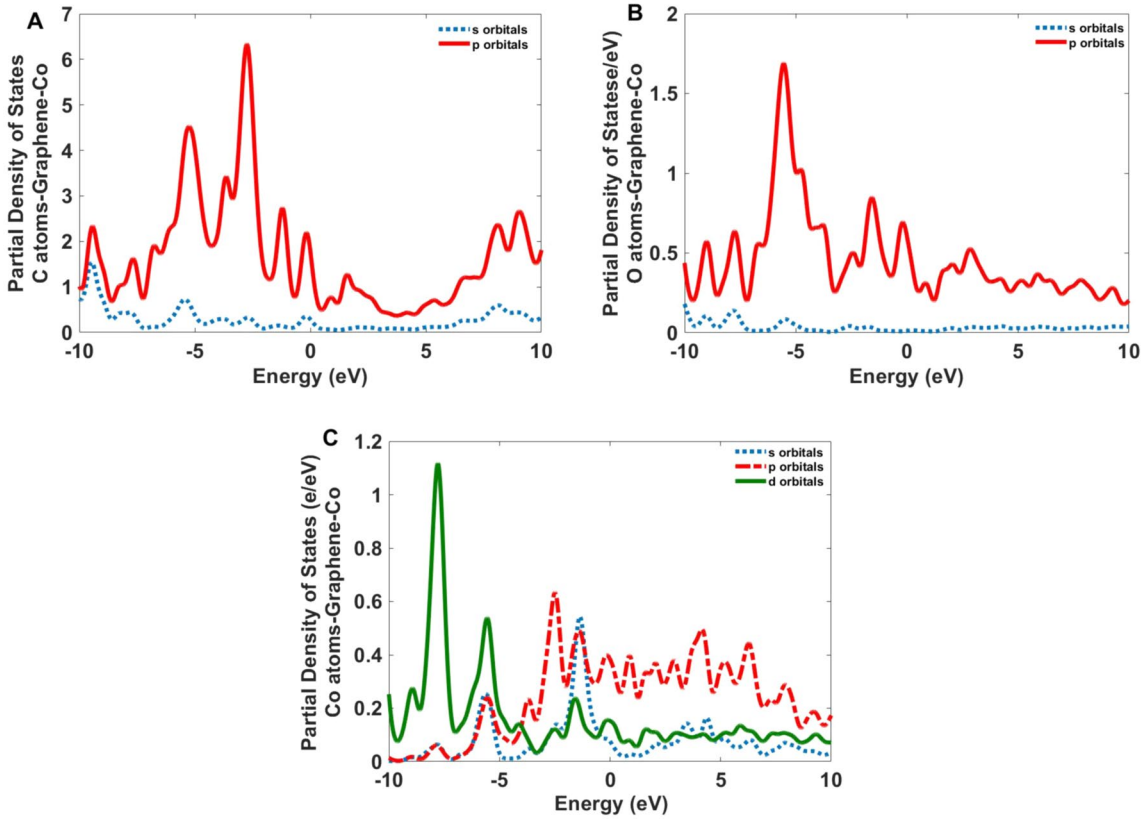

Figure 14. The partial density of states for the C, O, and Co atoms of the Co-GQDs.

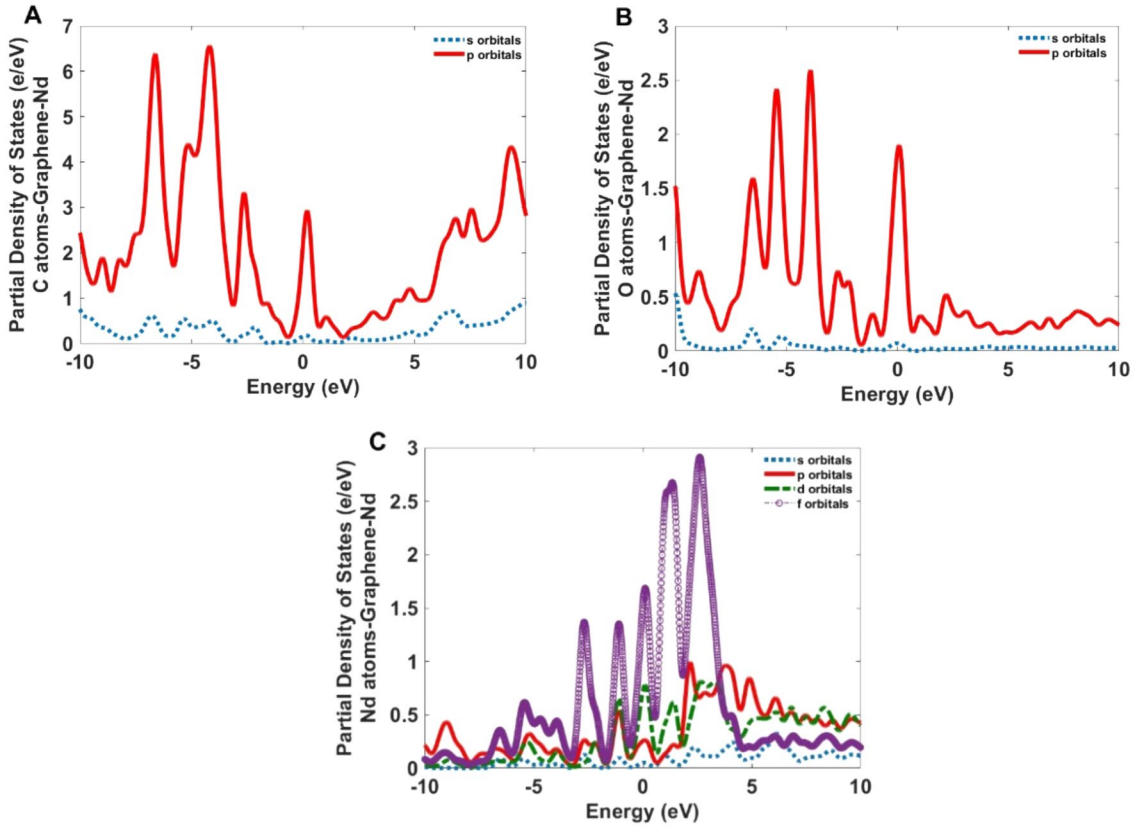

Figure 15. The partial density of states for the C, O, and Nd atoms of the Nd-GQDs.

Data availability

The datasets used and/or analyzed during the current study are available from the corresponding author upon reasonable request.

Received: 14 February 2023; Accepted: 22 June 2023
Published online: 24 June 2023

References

1. Xu, Y. *et al.* A novel controllable molecularly imprinted drug delivery system based on the photothermal effect of graphene oxide quantum dots. *J. Mater. Sci.* **54**, 9124–9139 (2019).
2. Nene, L. C., Managa, M. & Nyokong, T. Photo-physicochemical properties and in vitro photodynamic therapy activity of morpholine-substituted Zinc(II)-Phthalocyanines π–π stacked on biotinylated graphene quantum dots. *Dyes Pigment* **165**, 488–498 (2019).
3. Yue, J. *et al.* Facile design and development of photoluminescent graphene quantum dots grafted dextran/glycol-polymeric hydrogel for thermoresponsive triggered delivery of buprenorphine on pain management in tissue implantation. *J. Photochem. Photobiol. B.* **197**, 111530 (2019).
4. Ghafary, S. M., Nikkhah, M., Hatamie, S. & Hosseinkhani, S. Simultaneous gene delivery and tracking through preparation of photo-luminescent nanoparticles based on graphene quantum dots and chimeric peptides. *Sci. Rep.* **7**, 9552 (2017).
5. Havanur, S. *et al.* Poly(N,N-diethyl acrylamide)/functionalized graphene quantum dots hydrogels loaded with doxorubicin as a nano-drug carrier for metastatic lung cancer in mice. *Mater. Sci. Eng., C.* **105**, 110094 (2019).
6. Ju, J. & Chen, W. Graphene quantum dots as fluorescence probes for sensing metal ions: Synthesis and applications. *Curr. Org. Chem.* **19**, 1150–1162 (2015).
7. Fan, L. *et al.* Fluorescence resonance energy transfer quenching at the surface of graphene quantum dots for ultrasensitive detection of TNT. *Talanta* **101**, 192 (2012).
8. Ju, J. & Chen, W. In situ growth of surfactant-free gold nanoparticles on nitrogen-doped graphene quantum dots for electrochemical detection of hydrogen peroxide in biological environments. *Anal. Chem.* **87**, 1903–1910 (2015).
9. Li, Y. *et al.* Sequence-designed peptide nanofibers bridged conjugation of graphene quantum dots with graphene oxide for high-performance electrochemical hydrogen peroxide biosensor. *Adv. Mater. Interfaces* **4**, 1600895 (2017).
10. Soleymani, J., Hasanzadeh, M., Somi, M. H., Ozkan, S. A. & Jouyban, A. Targeting and sensing of some cancer cells using folate bioreceptor functionalized nitrogen-doped graphene quantum dots. *Int. J. Biol. Macromol.* **118**, 1021–1034 (2018).
11. Yang, Y. *et al.* A novel label-free electrochemical immune-sensor based on functionalized nitrogen-doped graphene quantum dots for carcinoembryonic antigen detection. *Biosens. Bioelectron.* **90**, 31–38 (2017).
12. Landry, M. P. *et al.* Single-molecule detection of protein efflux from microorganisms using fluorescent single-walled carbon nanotube sensor arrays. *Nat. Nanotechnol.* **12**, 368–377 (2017).
13. Song, H. *et al.* Preparation and biodistribution of 131I-labeled graphene quantum dots. *J. Radioanal. Nucl. Chem.* **316**, 685–690 (2018).
14. Rajender, G., Goswami, U. & Giri, P. K. Solvent-dependent synthesis of edge-controlled graphene quantum dots with high photoluminescence quantum yield and their application in confocal imaging of cancer cells. *J. Colloid Interface Sci.* **541**, 387–398 (2019).
15. Zhang, Q. *et al.* Cancer-targeting graphene quantum dots: Fluorescence quantum yields, stability, and cell selectivity. *Adv. Funct. Mater.* **29**, 1805860 (2019).
16. Wang, L. *et al.* Industrial production of ultra-stable sulfonated graphene quantum dots for Golgi apparatus imaging. *J. Mater. Chem. B* **5**, 5355–5361 (2017).
17. Kundu, S. *et al.* Enhancing the efficiency of DSSCs by the modification of TiO_2 photoanodes using N, F and S-codoped graphene quantum dots. *Electrochim. Acta.* **242**, 337–343 (2017).
18. Pan, D., Zhang, J., Li, Z. & Wu, M. Hydrothermal route for cutting graphene sheets into blue-luminescent graphene quantum dots. *Adv. Mater.* **22**, 734–738 (2010).
19. Yao, X. *et al.* Graphene Quantum dots-capped magnetic mesoporous silica nanoparticles as a multifunctional platform for controlled drug delivery, magnetic hyperthermia, and photothermal therapy. *Small* **13**, 1602225 (2017).
20. Chung, S., Revia, R. A. & Zhang, M. Graphene quantum dots and their applications in bioimaging, biosensing, and therapy. *Adv. Mater.* **33**, e1904362 (2019).
21. Alegret, N., Criado, A. & Prato, M. Recent advances of graphene-based hybrids with magnetic nanoparticles for biomedical applications. *Curr. Top. Med. Chem.* **24**, 529–536 (2017).
22. Justin, R. *et al.* Photoluminescent and superparamagnetic reduced graphene oxide–iron oxide quantum dots for dual-modality imaging, drug delivery, and photothermal therapy. *Carbon* **97**, 54–70 (2016).
23. Kuo, W. S. *et al.* Graphene quantum dots with nitrogen-doped content dependence for highly efficient dual-modality photodynamic antimicrobial therapy and bioimaging. *Biomaterials* **120**, 185–194 (2017).
24. Guo, M. *et al.* Ruthenium nitrosyl functionalized graphene quantum dots as an efficient nano platform for NIR-light-controlled and mitochondria-targeted delivery of nitric oxide combined with photothermal therapy. *Chem. Commun.* **53**, 3253–3256 (2017).
25. Xuan, Y. *et al.* Targeting N-doped graphene quantum dots with high photothermal conversion efficiency for dual-mode imaging and therapy in vitro. *Nanotechnology* **29**, 355101 (2018).
26. Fang, J. *et al.* Graphene quantum dots-gated hollow mesoporous carbon nano platform for targeting drug delivery and synergistic chemo-photothermal therapy. *Int. J. Nanomed.* **13**, 5991–6007 (2018).
27. Sun, H., Gao, N., Dong, K., Ren, J. & Qu, X. Graphene quantum dots-bandaids used for wound disinfection. *ACS Nano* **8**, 6202–6210 (2014).
28. Biswas, A. *et al.* Oxidant mediated one-step complete conversion of multi-walled carbon nanotubes to graphene quantum dots and their bioactivity against mammalian and bacterial cells. *J. Mater. Chem. B* **5**, 785–796 (2017).
29. Luo, Y. *et al.* Enhanced photocatalytic activity of sulfur-doped graphene quantum dots decorated with TiO_2 nanocomposites. *Mater. Res. Bull.* **97**, 428–435 (2018).
30. Ahmed, B. *et al.* Facile synthesis and photophysics of graphene quantum dots. *J. Photochem. Photobiol. A* **364**, 671–678 (2018).
31. Wu, C. *et al.* Construction of upconversion nitrogen-doped graphene quantum dots modified $BiVO_4$ photocatalyst with enhanced visible-light photocatalytic activity. *Ceram. Int.* **45**, 2088–2096 (2019).
32. Sun, L. *et al.* Role of Pyridinic-N for nitrogen-doped graphene quantum dots in oxygen reaction reduction. *J. Colloid Interface Sci.* **508**, 154–158 (2017).
33. Sajjadi, S., Khataee, A. & Kamali, M. Sonocatalytic degradation of methylene blue by a novel graphene quantum dots anchored CdSe nanocatalyst. *Ultrason. Sonochem.* **39**, 676–685 (2017).
34. Xu, T. *et al.* Graphitic carbon nitride co-modified by zinc phthalocyanine and graphene quantum dots for the efficient photocatalytic degradation of refractory contaminants. *Appl. Catal. B.* **244**, 96–106 (2019).

35. Wang, C. *et al.* In-situ synthesis and ultrasound enhanced adsorption properties of MoS_2/graphene quantum dot nanocomposite. *Chem. Eng. J.* **327**, 774–782 (2017).
36. Yao, Y., Guo, Y., Du, W., Tong, X. & Zhang, X. In situ synthesis of sulfur-doped graphene quantum dots decorated carbon nanoparticles hybrid as metal-free electrocatalyst for the oxygen reduction reaction. *J. Mater. Sci. Mater. Electron.* **29**, 17695–17705 (2018).
37. Riaz, R., Ali, M., Anwer, H., Ko, M. J. & Jeong, S. H. Highly porous self-assembly of nitrogen-doped graphene quantum dots over reduced graphene sheets for the photo-electrocatalytic electrode. *J. Colloid Interface Sci.* **557**, 174–184 (2019).
38. Majumder, T., Dhar, S., Chakraborty, P., Debnath, K. & Mondal, S. P. Advantages of ZnO nanotaper photoanodes in photoelectrochemical cells and graphene quantum dot sensitized solar cell applications. *J. Electroanal. Chem.* **813**, 92–101 (2018).
39. Huang, Y. *et al.* Graphene quantum dots-induced morphological changes in $CuCo_2S_4$ Nanocomposites for supercapacitor electrodes with enhanced performance. *Appl. Surf. Sci.* **463**, 498–503 (2019).
40. Qian, J. *et al.* Tailoring the electronic properties of graphene quantum dots by P doping and their enhanced performance in a metal-free composite photocatalyst. *J. Phys. Chem. C* **122**, 349–358 (2018).
41. Liu, T. *et al.* A graphene quantum dot decorated $SrRuO_3$ mesoporous film as an efficient counter electrode for high-performance dye-sensitized solar cells. *J. Mater. Chem. A.* **5**, 17848–17855 (2017).
42. Faridbod, F. & Sanati, A. L. Graphene quantum dots in electrochemical sensors/biosensors. *Curr. Anal. Chem.* **15**, 103–123 (2018).
43. Fan, Z., Li, S., Yuan, F. & Fan, L. Fluorescent graphene quantum dots for biosensing and bioimaging. *RSC Adv.* **5**, 19773–19789 (2015).
44. Hasanzadeh, M. & Shadjou, N. What are the reasons for the low use of graphene quantum dots in the immune-sensing of cancer biomarkers? *Mater. Sci. Eng. C* **71**, 1313–1326 (2017).
45. Mansuriya, B. D. Altintas, graphene quantum dot-based electrochemical immunosensors for biomedical applications. *Materials* **13**(1), 96 (2020).
46. Singh, A. K., Singh, R. S. & Singh, A. K. Recent developments in chemical doping of graphene using experimental approaches and its applications. *Adv. Eng. Mater.* **24**, 2200259 (2022).
47. Rezapour, M. R. Structural, electronic, and magnetic characteristics of graphitic carbon nitride nanoribbons and their applications in spintronics. *J. Phys. Chem. C* **126**(38), 16429–16436 (2022).
48. Ezawa, M. Quasi-ferromagnet spintronics in the graphene nanodisc–lead system. *New J. Phys.* **11**(9), 095005 (2009).
49. Yan, X., Cui, X., Li, B. & Li, L. S. Large, solution-processable graphene quantum dots as light absorbers for photovoltaics. *Nano Lett.* **10**(5), 1869–1873 (2010).
50. Kou, L., Li, F., Chen, W. & Guo, T. Synthesis of blue light-emitting graphene quantum dots and their application in flexible nonvolatile memory. *Org. Electron.* **14**(6), 1447–1451 (2013).
51. Shen, J., Zhu, Y., Yang, X. & Li, C. Graphene quantum dots: Emergent nano lights for bioimaging, sensors, catalysis, and photovoltaic devices. *Chem. Commun.* **48**(31), 3686–3699 (2012).
52. Geng, X. M. *et al.* Aqueous-processable noncovalent chemically converted graphene-quantum dot composites for flexible and transparent optoelectronic films. *Adv. Mater.* **22**, 638–642 (2010).
53. Zhu, S. J. *et al.* Strongly green-photoluminescent graphene quantum dots for bioimaging applications. *Chem. Commun.* **47**, 6858–6860 (2011).
54. Son, D. I. *et al.* Emissive ZnO-graphene quantum dots for white-light-emitting diodes. *Nat. Nanotechnol.* **7**, 465–471 (2012).
55. Konstantatos, G. *et al.* Hybrid graphene-quantum dot phototransistors with ultrahigh gain. *Nat. Nanotechnol.* **7**, 363–368 (2012).
56. Xu, H., Zhou, S., Fang, W. & Fan, Y. Synthesis of N-doped graphene quantum dots from bulk N-doped carbon nanofiber film for fluorescence detection of Fe^{3+} and ascorbic acid. *Fuller. Nanotub. Carbon Nanostruct.* **29**, 218 (2020).
57. Cheng, S. H. *et al.* All carbon-based photodetectors: An eminent integration of graphite quantum dots and two-dimensional graphene. *Sci. Rep.* **3**, 2694 (2013).
58. Bharathi, G. *et al.* Graphene quantum dot solid sheets: Strong blue-light-emitting & photocurrent-producing band-gap-opened nanostructures. *Sci. Rep.* **7**, 10850 (2017).
59. Guo, Z. *et al.* Facile synthesis of amine-functionalized graphene quantum dots with highly pH-sensitive photoluminescence. *Fuller. Nanotub. Carbon Nanostuct.* **25**, 704–709 (2017).
60. Liang, G. *et al.* Recent progress in the development of upconversion nanomaterials in bioimaging and disease treatment. *J. Nanobiotechnol.* **18**, 1–22 (2020).
61. Wen, G., Li, Z., Tong, C., Min, L. & Lu, Y. Extended near-infrared photoactivity of $Bi_6Fe_{1.9}Co_{0.1}Ti_3O_{18}$ by upconversion nanoparticles. *Nanomaterials* **8**, 534 (2018).
62. Chen, C. *et al.* Multi-photon near-infrared emission saturation nanoscopy using upconversion nanoparticles. *Nat. Commun.* **9**, 3290 (2018).
63. Dukhno, O. *et al.* Time-dependent luminescence loss of individual upconversion nanoparticles upon dilution in aqueous solutions. *Nanoscale* **10**, 15904–15910 (2018).
64. Ai, X. *et al.* Remote regulation of membrane channel activity by site-specific localization of lanthanide-doped upconversion nanocrystals. *Angew. Chem. Int. Ed.* **129**, 3077–3081 (2017).
65. Sun, M. *et al.* Phototherapy: Hierarchical plasmonic nanorods and upconversion core-satellite nano assemblies for multimodal imaging-guided combination phototherapy. *Adv. Mater.* **28**, 898–904 (2016).
66. Liang, L. *et al.* Facile assembly of functional upconversion nanoparticles for targeted cancer imaging and photodynamic therapy. *ACS Appl. Mater. Interfaces* **8**, 11945–11953 (2016).
67. Rao, L. *et al.* Erythrocyte membrane-coated upconversion nanoparticles with minimal protein adsorption for enhanced tumor imaging. *ACS Appl. Mater. Interfaces* **9**, 2159–2168 (2017).
68. Chen, G., Qiu, H., Prasad, P. N. & Chen, X. Upconversion nanoparticles: Design, nanochemistry, and applications in theranostics. *Chem. Rev.* **114**, 5161–5214 (2014).
69. Agrawal, A. *et al.* Localized surface plasmon resonance in semiconductor nanocrystals. *Chem Rev.* **118**, 3121–3207 (2018).
70. Chen, S. *et al.* Near-infrared deep brain stimulation via upconversion nanoparticle-mediated optogenetics. *Science* **359**, 679–683 (2018).
71. Du, P., Luo, L., Huang, X. & Yu, J. S. Ultrafast synthesis of bifunctional Er^{3+}/Yb^{3+}-codoped $NaBiF_4$ upconverting nanoparticles for nanothermometer and optical heater. *J. Colloid Interface Sci.* **514**, 172–181 (2018).
72. Qiu, Z., Shu, J. & Tang, D. Near-infrared-to-ultraviolet light-mediated photoelectrochemical aptasensing platform for cancer biomarker based on core-shell $NaYF_4$:Yb, Tm@TiO_2 upconversion micro rods. *Anal. Chem.* **90**, 1021–1028 (2018).
73. Wu, Z. *et al.* Highly efficient photocatalytic activity and mechanism of Yb^{3+}/Tm^{3+} codoped In_2S_3 from ultraviolet to near-infrared light towards chromium(VI) reduction and rhodamine B oxidative degradation. *Appl. Catal. B Environ.* **225**, 8–21 (2018).
74. Gu, B. & Zhang, Q. Recent advances on functionalized upconversion nanoparticles for detection of small molecules and ions in biosystems. *Adv. Sci.* **5**, 1700609 (2018).
75. Kim, D.-H. *et al.* High-efficiency electroluminescence and amplified spontaneous emission from a thermally activated delayed fluorescent near-infrared emitter. *Nat. Photonics.* **12**, 98 (2018).
76. Wang, W.-N. *et al.* Controlled synthesis of upconverting nanoparticles/$Zn_xCd_{1-x}S$ yolk-shell nanoparticles for efficient photocatalysis driven by NIR light. *Appl. Catal. B Environ.* **224**, 854–862 (2018).
77. Wen, S. *et al.* Advances in highly doped upconversion nanoparticles. *Nat. Commun.* **9**, 2415 (2018).

78. Zhao, J. *et al.* Upconversion luminescence-activated DNA nanodevice for ATP sensing in living cells. *J. Am. Chem. Soc.* **140**, 578–581 (2018).
79. Zhou, J. *et al.* Activation of the surface dark-layer to enhance upconversion in a thermal field. *Nat. Photon.* **12**, 154 (2018).
80. Zhang, Y. *et al.* Near-infrared-triggered antibacterial and antifungal photodynamic therapy based on lanthanide-doped upconversion nanoparticles. *Nanoscale* **10**, 15485–15495 (2018).
81. Boyer, J.-C., Vetrone, F., Cuccia, L. A. & Capobianco, J. A. Synthesis of colloidal upconverting $NaYF_4$ nanocrystals doped with Er^{3+}, Yb^{3+} and Tm^{3+}, Yb^{3+} via thermal decomposition of lanthanide trifluoroacetate precursors. *J. Am. Chem. Soc.* **128**, 7444–7445 (2006).
82. Zhang, K. K. *et al.* Nanodiamonds conjugated upconversion nanoparticles for bio-imaging and drug delivery. *J. Colloid Interface Sci.* **537**, 316–324 (2019).
83. Li, X. M., Zhang, F. & Zhao, D. Y. Lab on upconversion nanoparticles: Optical properties and applications engineering via designed nanostructure. *Chem. Soc. Rev.* **44**, 1346–1378 (2015).
84. Xiang, J. *et al.* Antigen-loaded upconversion nanoparticles for dendritic cell stimulation, tracking, and vaccination in dendritic cell-based immunotherapy. *ACS Nano* **9**, 6401–6411 (2015).
85. Xu, J. *et al.* Near-infrared-triggered photodynamic therapy with multitasking upconversion nanoparticles in combination with checkpoint blockade for immunotherapy of colorectal cancer. *ACS Nano* **11**, 4463–4474 (2017).
86. Wang, X. *et al.* Bioinspired drug delivery carrier for enhanced tumor-targeting in melanoma mice model. *J. Biomed. Nanotechnol.* **15**, 1482–1491 (2019).
87. Chang, S. L. Microwave sol–gel derived $NaCaGd(MoO_4)_3$: Er^{3+}/Yb^{3+} phosphors and their upconversion photoluminescence properties. *Infrared Phys. Technol.* **76**, 353–359 (2016).
88. Peng, D., Huang, X. & Yu, J. S. Yb^{3+}-concentration dependent upconversion luminescence and temperature sensing behavior in Yb^{3+}/Er^{3+} codoped Gd_2MoO_6 nanocrystals prepared by a facile citric-assisted Sol-Gel method. *Inorg. Chem. Front.* **4**, 1987–1995 (2017).
89. Guan, Y. *et al.* Near-infrared triggered upconversion polymeric nanoparticles based on aggregation-induced emission and mitochondria targeting for photodynamic cancer therapy. *ACS Appl. Mater. Interfaces.* **9**, 26731–26739 (2017).
90. Zhao, N., Wu, B., Hu, X. & Xing, D. NIR-triggered high-efficient photodynamic and chemo-cascade therapy using caspase-3 responsive functionalized upconversion nanoparticles. *Biomaterials* **141**, 40–49 (2017).
91. Placha, D. & Jampilek, J. Graphenic materials for biomedical applications. *Nanomaterials* **9**(1758), 73 (2019).
92. Maiti, D., Tong, X. M., Mou, X. Z. & Yang, K. Carbon-based nanomaterials for biomedical applications: A recent study. *Front. Pharmacol.* **9**, 1401 (2019).
93. Ghosal, K. & Sarkar, K. Biomedical applications of graphene nanomaterials and beyond. *ACS Biomater. Sci. Eng.* **4**, 2653–2703 (2018).
94. Wang, S., Chen, Z. G., Cole, I. & Li, Q. Structural evolution of graphene quantum dots during thermal decomposition of citric acid and the corresponding photoluminescence. *Carbon* **82**, 304–313 (2015).
95. Ashouri, S., Dolatyari, M., Zarghami, A., Farshbaf Pourabad, R. & Rostami, A. Effects of Ag/SiO_2 nanoparticles on gene expression of digestive α-amylase in Colorado potato beetle. *Austin J. Biotechnol. Bioeng.* **9**, 1116–1126 (2022).
96. Biswal, B. P., Shinde, D. B., Pillai, V. K. & Banerjee, R. Stabilization of graphene quantum dots (GQDs) by encapsulation inside zeolitic imidazolate framework nanocrystals for photoluminescence tuning. *Nanoscale* **5**(21), 10556–10561 (2013).
97. Shen, J., Zhu, Y., Chen, C., Yang, X. & Li, C. Facile preparation and upconversion luminescence of graphene quantum dots. *Chem. Commun.* **47**, 2580–2582 (2011).
98. Mhlongo, M. R., Koao, L. F., Motaung, T. E., Kroon, R. E. & Motloung, S. V. analysis of Nd^{3+} concentration on the structure, morphology, and photoluminescence of sol–gel $Sr_3ZnAl_2O_7$ nano phosphor. *Results Phys.* **12**, 1786–1796 (2019).

Acknowledgements

The study has been supported by the ASEPE Company, Tabriz, Iran.

Author contributions

A.Z. performed simulations and revised the manuscript. M.D. conceived the basic idea of the doping part and performed the simulations, synthesized the QDs, and wrote the manuscript. A.R. conceived the basic idea, characterized the QDs, supervised the project, and revised the manuscript. H.M. supervised the project and revised the manuscript.

Competing interests

The authors declare no competing interests.

Additional information

Correspondence and requests for materials should be addressed to A.R.

Reprints and permissions information is available at www.nature.com/reprints.

Publisher's note Springer Nature remains neutral with regard to jurisdictional claims in published maps and institutional affiliations.